Static Friction in a Robot Joint – Modeling and Identification of Load and Temperature Effects

André Carvalho Bittencourt*

Student
Division of Automatic Control
Department of Electrical Engineering
Linköping University
Linköping, Sweden
Email: andrecb@isy.liu.se

Svante Gunnarsson

Professor
Division of Automatic Control
Department of Electrical Engineering
Linköping University
Linköping, Sweden
Email: svante@isy.liu.se

Friction is the result of complex interactions between contacting surfaces in a nanoscale perspective. Depending on the application, the different models available are more or less suitable. Available static friction models are typically considered to be dependent only on relative speed of interacting surfaces. However, it is known that friction can be affected by other factors than speed.

In this paper, the typical friction phenomena and models used in robotics are reviewed. It is shown how such models can be represented as a sum of linear and nonlinear functions of relevant states, and how the identification method described in [1] can be used to identify them when all states are measured. The discussion follows with a detailed experimental study of friction in a robot joint under changes of joint angle, load torque and temperature. Justified by their significance, load torque and temperature are included in an extended static friction model. The proposed model is validated in a wide operating range, considerably improving the prediction performance compared to a standard model.

1 Introduction

Friction exists in all mechanisms to some extent. It can be defined as the tangential reaction force between two surfaces in contact. It is a nonlinear phenomenon which is physically dependent on contact geometry, topology, properties of the materials, relative velocity, lubricant, etc. [2]. Friction has been constantly investigated by researchers due to its importance in several fields [3]. In this paper, friction has been studied based on experiments on an industrial robot.

One reason for the interest in friction of manipulator joints is the need to model friction for control purposes [4–8], where a precise friction model can considerably improve the overall performance of a manipulator with respect to accuracy and control stability. Since friction can relate to the wear down process of mechanical systems [9], including robot joints [10], there is also interest in friction modeling for robot condition monitoring and fault detection [10–17].

A friction model consistent with real experiments is necessary for successful simulation, design and evaluation. Due to the complexity of friction, it is however often difficult to obtain models that can describe all the empirical observations (see [2] for a comprehensive discussion on friction physics and first principle friction modeling). In a robot joint, the complex interaction of components such as gears, bearings and shafts which are rotating/sliding at different velocities, makes physical modeling difficult. An example of an approach to model friction of complex transmissions can be found in [18], where the author designs joint friction models based on physical models of elementary joint components as helical gear pairs and pre-stressed roller bearings.

Empirically motivated friction models have been successfully used in many applications, including robotics [6, 19–

*This work was supported by ABB and the Vinnova Industry Excellence Center LINK-SIC at Linköping University.

21]. This category of models was developed through time according to empirical observations of the phenomenon [3]. Considering a set of states, $\mathcal{X}$, and parameters, θ, these models can be described as the sum of M functions f_j that describe the behavior of friction, $\mathcal{F}$,

$$\mathcal{F}(\mathcal{X},\theta) = \sum_{j=1}^{M} f_j(\mathcal{X},\theta). \qquad (\mathcal{M})$$

The choice $\mathcal{X} = [z, \dot{q}, q]$, where z is an internal state related to the dynamic behavior of friction, q is a generalized coordinate and $\dot{q} = \frac{\mathrm{d}}{\mathrm{d}t}q$, gives the set of Generalized Empirical Friction Model structures (GEFM) [2].

Among the GEFM model structures, the LuGre model [6, 20] is a common choice in the robotics community. For a revolute joint, it can be described as

$$\begin{aligned} \tau_f &= \sigma_0 z + \sigma_1 \dot{z} + h(\dot{\varphi}) \qquad (\mathcal{M}_L) \\ \dot{z} &= \dot{\varphi} - \sigma_0 \frac{|\dot{\varphi}|}{g(\dot{\varphi})} z, \end{aligned}$$

where τ_f is the friction torque, φ is the joint motor angle and $\dot{\varphi} = \frac{\mathrm{d}}{\mathrm{d}t}\varphi$. The state z is related to the dynamic behavior of asperities in the interacting surfaces and can be interpreted as their average deflection, with stiffness σ_0 and damping σ_1.

The function $h(\dot{\varphi})$ represents the velocity strengthening (viscous) friction and is dependent on the stress versus strain rate relationship. For Newtonian fluids, the shear stress follows a linear dependency to the shear rate $\tau = \mu \frac{\mathrm{d}}{\mathrm{d}y}u$, where τ is the shear stress, μ is the viscosity and $\frac{\mathrm{d}u}{\mathrm{d}y}$ is the velocity gradient perpendicular to the direction of shear. It is typical to consider a Newtonian behavior, yielding the relationship

$$h(\dot{\varphi}) = F_v \dot{\varphi}$$

for the viscous behavior of friction.

The function $g(\dot{\varphi})$ captures the velocity weakening of friction. Motivated by the observations mainly attributed to Stribeck [22–24], $g(\dot{\varphi})$ is usually modeled as

$$g(\dot{\varphi}) = F_c + F_s e^{-\left|\frac{\dot{\varphi}}{\dot{\varphi}_s}\right|^{\alpha}},$$

where F_c is the Coulomb friction, F_s is defined as the standstill friction parameter[1], $\dot{\varphi}_s$ is the Stribeck velocity and α is the exponent of the Stribeck nonlinearity. The model structure $\mathcal{M}_L$ is a GEFM with $\mathcal{X} = [z, \dot{\varphi}]$ and $\theta = [\sigma_0, \sigma_1, F_c, F_s, F_v, \dot{\varphi}_s, \alpha]$. According to [20] it can successfully describe many of the friction characteristics.

[1] F_s is commonly called static friction. An alternative nomenclature was adopted to make a distinction between the dynamic/static friction phenomena.

Since z is not measurable, a difficulty with $\mathcal{M}_L$ is the estimation of the dynamic parameters $[\sigma_0, \sigma_1]$. In [6], these parameters are estimated in a robot joint by means of open loop experiments and by use of high resolution encoders. Open-loop experiments are not always possible, and it is common to accept only a static description of $\mathcal{M}_L$. For constant velocities, $\mathcal{M}_L$ is equivalent to the static model $\mathcal{M}_S$:

$$\tau_f(\dot{\varphi}) = g(\dot{\varphi})\mathrm{sign}(\dot{\varphi}) + h(\dot{\varphi}) \qquad (\mathcal{M}_S)$$

which is fully described by the g- and h functions. In fact, $\mathcal{M}_L$ simply adds dynamics to $\mathcal{M}_S$. The typical choice for g and h, as defined previously for $\mathcal{M}_L$, yields the static model structure $\mathcal{M}_0$:

$$\tau_f(\dot{\varphi}) = \left[F_c + F_s e^{-\left|\frac{\dot{\varphi}}{\dot{\varphi}_s}\right|^{\alpha}} \right] \mathrm{sign}(\dot{\varphi}) + F_v \dot{\varphi}. \qquad (\mathcal{M}_0)$$

$\mathcal{M}_0$ requires a total of 4 parameters to describe the velocity weakening regime $g(\dot{\varphi})$ and 1 parameter to capture viscous friction $h(\dot{\varphi})$. See Fig. 3 for an interpretation of the parameters.

From empirical observations, it is known that friction can be affected by several factors,

temperature,	velocity,
force/torque levels,	acceleration,
position,	lubricant properties.

A shortcoming of the LuGre model structure, as with any GEFM, is the dependence only of the states $\mathcal{X} = [z, \dot{q}, q]$. In more demanding applications, the effects of the remaining variables can not be neglected. In [25], the author observes a strong temperature dependence, while in [6] joint load torque and temperature are considered as disturbances and estimated in an adaptive framework. In [26, 27], the effects of load are modeled as a linear effect on F_c in a model structure similar to $\mathcal{M}_0$. In the recent contribution of [28] the load effects are revisited to include also a linear dependency on F_s. However, more work is needed in order to understand the influence of different factors on the friction properties. A more comprehensive friction model is needed to improve tasks related to design, simulation and evaluation for machines with friction.

The objective of this paper is to analyze and model the effects in static friction related to joint angle, load torques and temperature. The phenomena are observed in joint 2 of an ABB IRB 6620 industrial robot, see Fig. 1(a). Two load torque components are examined, the torque aligned to the joint *DoF* (degree of freedom) and the torque perpendicular to the joint *DoF*. These torques are in the paper named manipulation torque τ_m and perpendicular torque τ_p, see Fig. 1(b).

By means of experiments, these variables are analyzed and modeled based on the empirical observations. The task of modeling is to find a suitable model structure according

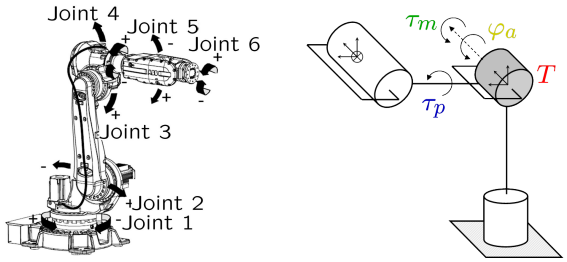

(a) ABB IRB 6620 robot with 150 kg payload and 2.2 m reach.

(b) Schematics of the 3 first joints including the torque definitions for joint 2.

Fig. 1. The experiments were made on joint 2 of the ABB robot IRB 6620. φ_a is the joint angle, T the joint temperature, τ_m the manipulation torque and τ_p the perpendicular torque.

to:

$$\tau_f(\mathcal{X}^*,\theta) = \sum_{j=1}^{M} f_j(\mathcal{X}^*,\theta) \qquad (\mathcal{M}^*)$$
$$\mathcal{X}^* = [\dot{\varphi}, \varphi_a, \tau_p, \tau_m, T],$$

where T is the joint (more precisely, lubricant) temperature and φ_a the joint angle at the arm side.

Ideally, the chosen model should be coherent with the empirical observations and, simultaneously, with the lowest dimension of θ, the parameter vector, and with the lowest number of describing functions (minimum M). For practical purposes, the choice of f_i should also be suitable for a useful identification procedure.

The work presented here is based in [29], where a friction model was proposed to describe the effects of load and temperature in a robot joint. More detailed analysis of the modeling assumptions are presented, together with a more general framework for identification of friction models. The paper is organized as follows. Section 2 presents the method used to estimate static friction levels in a robot joint and consequently its friction curve, an identification procedure is also described for general parametric description of friction curves and some model simplifications are justified. Section 3 contains the major contribution of this paper, with the empirical analysis, modeling and validation. Conclusions and future work are presented in Section 4.

2 Static Friction Curve

Static friction is typically presented in a *friction curve*, a plot of static friction levels against speed. It is related to the Stribeck curve under the simplification that viscosity and contact pressure are constant. An example of a friction curve estimated in a robot joint can be seen in Fig. 3.

From a phenomenological perspective, a friction curve can be divided into three regimes, according to the lubrication characteristics: *boundary (BL), mixed (ML) and elasto-hydrodynamic lubrication (EHL)*. The phenomena present in very low velocities (BL) is mostly related to interactions between the asperities of the surfaces in contact. With the increase of velocity, there is a consequent increase of the lubrication film between the surfaces and a decrease of friction (ML) until it reaches a full lubrication profile (EHL) with a total separation of the surfaces by the lubricant. In EHL, friction is proportional to the force needed to shear the lubricant layer, thus dependent on the lubricant properties, specially viscosity. Recalling the static friction model $\mathcal{M}_S$, the BL and ML regimes are described by the velocity weakening function $g-$ and the EHL regime is described by $h-$.

In this section, an experimental procedure is suggested to estimate static friction levels at constant speeds in a robot joint and consequently its friction curve. Given static friction estimates, it is shown how the general friction model $\mathcal{M}$ can be identified with the method described in [1], when the states $\mathcal{X}$ are available. Finally, the model structure $\mathcal{M}_0$ is simplified to achieve a minimal description of static friction.

2.1 Estimation Procedure

A manipulator is a multivariable, nonlinear system that can be described in a general manner through the rigid multi body dynamic model

$$M(\varphi)\ddot{\varphi} + C(\varphi,\dot{\varphi}) + \tau_g(\varphi) + \tau_f(\dot{\varphi}) = u, \qquad (1)$$

where $M(\varphi)$ is the inertia matrix, $C(\varphi,\dot{\varphi})$ relates to speed dependent terms (e.g. Coriolis and centrifugal), $\tau_g(\varphi)$ are the gravity-induced joint torques and τ_f contains the joint friction components. The system is controlled by the input torque, u, applied by the joint motor (in the experiments the torque reference from the servo was measured[2]).

For single joint movements ($C(\varphi,\dot{\varphi})=0$) under constant speed ($\ddot{\varphi}\approx 0$), Eq. (1) simplifies to

$$\tau_g(\varphi) + \tau_f = u. \qquad (2)$$

The resulting applied torque u drives only friction and gravity-induced torques. The required torques to drive a joint in forward, u^+, and reverse, u^-, directions at the constant speed level $\bar{\dot{\varphi}}$ and at a joint angle value $\bar{\varphi}$ (so that $\tau_g(\bar{\varphi})$ is equal in both directions), are

$$\tau_f(\bar{\dot{\varphi}}) + \tau_g(\bar{\varphi}) = u^+ \qquad (3a)$$
$$\tau_f(-\bar{\dot{\varphi}}) + \tau_g(\bar{\varphi}) = u^-. \qquad (3b)$$

In the case an estimate of $\tau_g(\bar{\varphi})$ is available, it is possible to isolate the friction component in each directions using Eq. (3). If such estimate is not possible (e.g. not all masses are completely known), τ_f can still be achieved in the case

[2] It is known that using the torque reference from the servo as a measure of the joint torque might not always hold because of the temperature dependence of the torque constant of the motors. The deviations are however considered to be small and are neglected during the experiments.

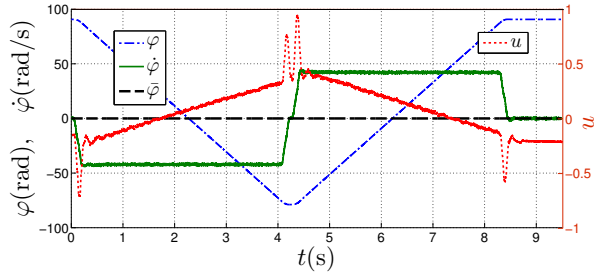

Fig. 2. Excitation signals used for the static friction estimation at $\bar{\varphi}=42$ rad/s.

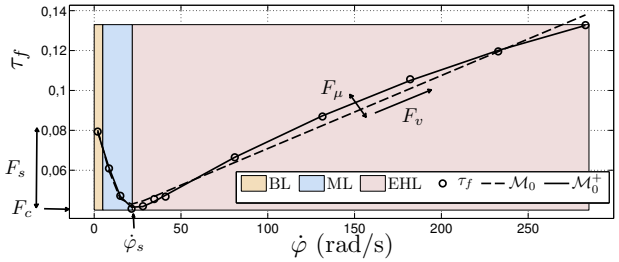

Fig. 3. Static friction curve with lubrication regimes and model-based predictions. Circles indicate friction levels achieved using Eq. (4).

that τ_f is independent of the rotation direction. Subtracting the equations yields

$$\tau_f(\bar{\dot{\varphi}}) - \tau_f(-\bar{\dot{\varphi}}) = u^+ - u^-$$

and if $\tau_f(-\bar{\dot{\varphi}}) = -\tau_f(\bar{\dot{\varphi}})$, the resulting *direction independent friction* is:

$$\tau_f(\bar{\dot{\varphi}}) = \frac{u^+ - u^-}{2}. \tag{4}$$

In the experiments, each joint is moved separately with the desired speed in both directions around a given joint angle $\bar{\varphi}$. Fig. 2 shows the measured joint angle-, speed- and torque[3] signals sampled at 2 kHz[4] for $\bar{\dot{\varphi}}=42$ rad/s around $\bar{\varphi}=0$. The constant speed data is segmented around $\bar{\varphi}$ and the static friction levels can be achieved using Eq. (3) or (4).

The procedure can be repeated for several different speeds and a friction curve can be drawn. As shown in [29], there is only a small direction dependency of friction for the investigated joint. Therefore, in this paper, friction levels are achieved using Eq. (4), which is not influenced by deviations in the gravity model of the robot.

[3]Throughout the paper all torques are normalized to the maximum manipulation torque at low speed.

[4]Similar results have been experienced with sampling rates down to 220 Hz.

2.2 General Parametric Description and Identification

The general friction models described by $\mathcal{M}$, can be written as

$$\hat{\tau}_f(\mathcal{X}_i, \theta) = \sum_{j=1}^{N_\eta} f_j(\mathcal{X}_i, \rho)\eta_j. \tag{5}$$

where the index i relates to the i-th measurement in the data set. The parameters vector $\theta = \left[\eta^T, \rho^T\right]^T$ has dimension $(N_\eta + N_\rho)$ and is divided according to the manner they appear in the model, respectively linearly/nonlinearly. Notice that if there are no linear parameters, i.e. η is empty, (5) reads directly as $\mathcal{M}$ by taking $\theta = \rho$. As it will be shown, the structure of (5), can be exploited when defining an identification method.

Considering a total of N measurements, the residuals (innovations) between predictions and measurements are written as $\varepsilon(i,\theta) = \tau_f(i) - \hat{\tau}_f(\mathcal{X}_i, \theta)$. For the following discussion, it is assumed that $\mathcal{X}_i$ is available so that it is possible to construct $f_j(\mathcal{X}_i, \rho)$.

The identification objective can be formulated as a least squares

$$\hat{\theta} = \arg\min_\theta \sum_{i=1}^{N} \varepsilon^2(i,\theta), \tag{6}$$

and the objective is to minimize the sum of squared errors. The minimum of (6) occurs where the gradient of the innovations, $\psi(i,\theta) = \frac{\partial}{\partial\theta}\varepsilon(i,\theta)$, is zero. For the model in (5), this gradient takes the form

$$\psi(i,\theta) = \Big[f_1(\mathcal{X}_i,\theta), \cdots, f_{N_\eta}(\mathcal{X}_i,\theta), \tag{7}$$

$$\frac{\partial}{\partial\rho_1}\hat{\tau}_f(\mathcal{X}_i,\theta), \cdots \frac{\partial}{\partial\rho_{N_\rho}}\hat{\tau}_f(\mathcal{X}_i,\theta)\Big]^T, \tag{8}$$

where it is easy to realize the separable nature of the model. The solution for ρ can not be found explicitly, but can be solved numerically using an optimization routine. For instance, if η is empty, gradient based methods can be used to find an estimate of ρ [30].

As presented in [1], the separable structure of the model can be explored. Defining the matrix $\{\mathbf{f}(\rho)\}_{i,j} = f_j(\mathcal{X}_i,\rho)\eta_j$, for any given ρ, the solution for η, is given by the least squares solution

$$\hat{\eta} = \mathbf{f}^\dagger(\rho)\tau_f, \quad \mathbf{f}^\dagger(\rho) = \{\mathbf{f}^T(\rho)\mathbf{f}(\rho)\}^{-1}\mathbf{f}^T(\rho) \tag{9}$$

where τ_f denotes here the vector of measurements $\{\tau_f(i)\}_1^N$ and $\mathbf{f}^\dagger(\rho)$ is the Moore-Penrose pseudoinverse [1]. Substituting this back in (6), the problem can be rewritten as a function only of ρ

$$\hat{\rho} = \arg\min_\rho \; ||\tau_f - \mathbf{f}(\rho)\hat{\eta}||^2 = \arg\min_\rho \; ||P^\perp_{\mathbf{f}(\rho)}\tau_f||^2, \tag{10}$$

where $P^{\perp}_{\mathbf{f}(\rho)} = I - \mathbf{f}(\rho)\mathbf{f}^{\dagger}(\rho)$ is the projector on the orthogonal complement of the column space of $\mathbf{f}(\rho)$. The idea is then to first find $\hat{\rho}$, and then plug it back in (9) to find $\hat{\eta}$. This illustrates the algorithm proposed in [1], where it is also shown that the resulting point $\hat{\theta} = [\hat{\eta}^T, \hat{\rho}^T]^T$ minimizes (6).

There is, however, no closed form solution to (10). An approach is to consider gradient based methods where information of the gradient of $P^{\perp}_{\mathbf{f}(\rho)}\tau_f$ is relevant. In [1], it is shown that the gradient of $P^{\perp}_{\mathbf{f}(\rho)}\tau_f$ requires only computation of derivatives of $\mathbf{f}(\rho)$, as in (8), see [1] for a detailed treatment. In this work, a 2-step identification procedure is used, in a initial step, a coarse grid search is used to find initial estimates of ρ. The problem (10) is then solved given the initial estimates using a trust-region reflective algorithm available in the Matlab's Optmization Toolbox. The resulting $\hat{\rho}$ estimate is finally used to find $\hat{\eta}$ as is in (9).

To assess the resulting performance of the identification procedure, it is possible to provide an estimate of the identified parameters uncertainties. For any unbiased estimator, the following relationship for its covariance Σ_{θ_N} holds, [30],

$$\Sigma_{\theta_N} \geq \kappa_0 \left[\sum_{i=1}^{N} E\psi(i,\theta)\psi^T(i,\theta) \right]^{-1} = \Sigma^*_{\theta_N} \qquad (11)$$

where for Gaussian innovations with variance λ_0, $\kappa_0 = \lambda_0$, [30]. Under this assumption, given an estimate $\hat{\theta}_N$ of θ after N observations, $\Sigma^*_{\theta_N}$ can be estimated from the data as

$$\hat{\Sigma}^*_{\theta_N} = \hat{\lambda}_N \left[\frac{1}{N} \sum_{i=1}^{N} \psi(i,\hat{\theta}_N)\psi^T(i,\hat{\theta}_N) \right]^{-1} \qquad (12)$$

$$\hat{\lambda}_N = \frac{1}{N} \sum_{i=1}^{N} \varepsilon^2(i,\hat{\theta}_N). \qquad (13)$$

The quantity in (12) is used throughout this work as a covariance estimate for $\hat{\theta}$.

For the model structure $\mathcal{M}_0$ in the first quadrant, Eq. (5) can be written as

$$\mathcal{X} = \dot{\varphi}, \quad \mathbf{f}(\dot{\varphi},\rho) = \left[1,\ e^{-\left|\frac{\dot{\varphi}}{\dot{\varphi}_s}\right|^{\alpha}},\ \dot{\varphi} \right]$$
$$\eta = [F_c,\ F_s,\ F_v], \quad \rho = [\dot{\varphi}_s,\ \alpha].$$

The model parameters are identified using the direction independent data (circles) in Fig. 3. The resulting identified parameters values are shown in Table 1 with one standard deviation. The dashed line in Fig. 3 is obtained by model-based predictions of the resulting model, with sum of absolute prediction errors no more than $3.0\,10^{-2}$.

A closer investigation of the friction curve in Fig. 3 reveals that the behavior of friction at high speeds is slightly nonlinear with speed. This feature is related to the non-Newtonian behavior of the lubricant at high speeds [25]. In this case, the fluid presents a pseudoplastic behavior, with a decrease of the apparent viscosity (increase of friction) with share rate (joint speed). The behavior motivates the suggestion of an alternative model structure

$$\tau_f(\dot{\varphi}) = F_c + F_s e^{-\left|\frac{\dot{\varphi}}{\dot{\varphi}_s}\right|^{\alpha}} + F_v\dot{\varphi} + F_\mu\dot{\varphi}^{\beta}, \qquad (\mathcal{M}_0^+)$$

where F_μ and β relates to the non-Newtonian part of the viscous friction behavior and capture the deviation from a Newtonian behavior. The parameters are identified for the friction curve in Fig. 3. The resulting predictions are shown by the solid line in Fig. 3, with sum of absolute prediction error as $5.5\,10^{-3}$.

This example illustrates that it might be worth to consider the non-Newtonian behavior of the lubricant in applications where high accuracy is needed at high speeds. However, for simplicity, this behavior is not considered further in this paper.

2.3 Fixing α

Despite the non-Newtonian behavior of the lubricant, the model $\mathcal{M}_0$ represents well the behavior of static friction with speed. From a practical perspective, it is desirable to achieve a minimal number of parameters and avoid nonlinear terms which are costly to identify.

Following the general static friction description $\mathcal{M}_S$, the model $\mathcal{M}_0$ represents the decrease of friction in the velocity weakening regime, g, through the term $e^{-\left|\frac{\dot{\varphi}}{\dot{\varphi}_s}\right|^{\alpha}}$. The term takes two nonlinear parameters, α and $\dot{\varphi}_s$. It is common to accept α as a constant between 0.5 and 2 [6,8,20]. As seen in Fig. 4, $\dot{\varphi}_s$ changes the constant of the decay while α changes its curvature. Notice from Fig. 4(a) and Fig. 4(b) that small choices of α can considerably affect friction at high speeds, which is not desirable. For these reasons, α is fixed as presented next.

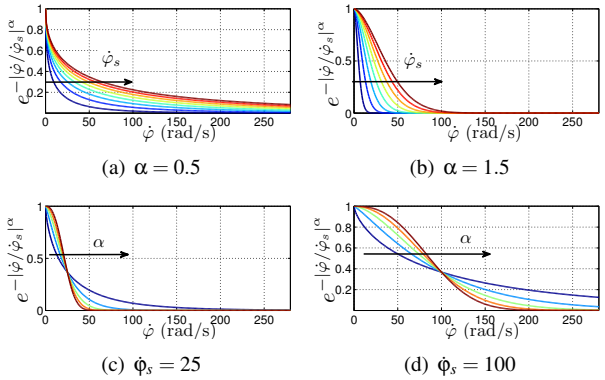

(a) $\alpha = 0.5$ (b) $\alpha = 1.5$

(c) $\dot{\varphi}_s = 25$ (d) $\dot{\varphi}_s = 100$

Fig. 4. Illustration of effects in the velocity weakening regime caused by $\dot{\varphi}_s$ and α. Figures (a) and (b) with $\dot{\varphi}_s = [1, 50]$ rad/s. Figures (c) and (d) with $\alpha = [0.02, 3.00]$.

Table 1. Identified $\mathcal{M}_0$ parameters for the data shown in Fig. 3.

$F_c\,[10^{-2}]$	$F_s\,[10^{-2}]$	$F_v\,[10^{-4}]$	$\dot{\varphi}$	α
3.4 ± 0.176	4.6 ± 0.48	3.68 ± 0.12	10.68 ± 1.08	1.93 ± 0.60

Considering all static friction data presented in this work, in a total of 488 friction curves with more than 5800 samples, α is chosen as the value minimizing Eq. (6) for the model structure $\mathcal{M}_0$ when all other parameters are free at each friction curve. Fig 5 presents the resulting relative increase in the cost for different values of α. The value at minimal cost is $\alpha^* = 1.36 \pm 0.011$.

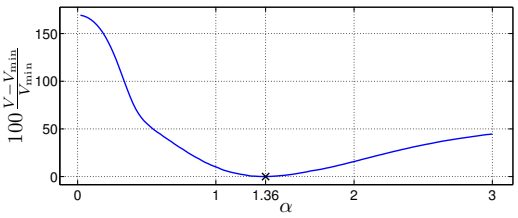

Fig. 5. Relative cost increase as a function of α for the model structure $\mathcal{M}_0$.

3 Empirically Motivated Modeling

Using the described static friction curve estimation method, it is possible to design a set of experiments to analyze how the states $\mathcal{X}^*$ affect static friction. As shown in Section 2.2, the model structure $\mathcal{M}_0$ can represent static friction dependence on $\dot{\varphi}$ fairly well. $\mathcal{M}_0$ is therefore taken as a primary choice, with α fixed at $\alpha^* = 1.36$. Whenever a single instance of $\mathcal{M}_0$ can not describe the observed friction behavior, extra terms $f_j(\mathcal{X}^*, \theta)$ are proposed and included in $\mathcal{M}_0$ to achieve a satisfactory model structure $\mathcal{M}^*$.

3.1 Guidelines for the Experiments

In order to be able to build a friction model including more variables than the velocity, it is important to separate their influences. The situation is particularly critical regarding temperature as it is difficult to control it inside a joint. Moreover, due to the complex structure of an industrial robot, changes in joint angle might move the mass center of the robot arm system, causing variations of joint load torques. To avoid undesired effects, the guidelines below were followed during the experiments.

3.1.1 Isolating Joint Load Torque Dependency from Joint Angle Dependency

Using an accurate dynamic robot model[5], it is possible to predict the joint torques for any given robot configuration (a set of all joints angles). For example, Fig. 6 shows the resulting τ_m and τ_p at joint 2, related to variations of joint 2 and 4 angles ($\varphi_{a,2}$ and $\varphi_{a,4}$) throughout their workrange. Using

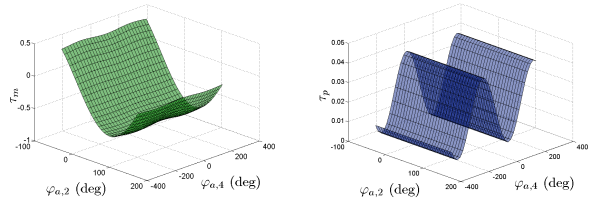

(a) Simulated τ_m (b) Simulated τ_p

Fig. 6. Simulated joint load torques at joint 2 caused by angle variations of joints 2 and 4, $\varphi_{a,2}$ and $\varphi_{a,4}$ respectively. Notice the larger absolute values for τ_m when compared τ_p.

this information, a set of configurations *can be selected a priori* in which it is possible to estimate parameters in an efficient way.

3.1.2 Isolating Temperature Effects

Some of the experiments require that the temperature of the joint is under control. Using joint lubricant temperature measurements[6], the joint thermal decay constant κ was estimated to 3.04 h. Executing the static friction curve identification experiment periodically, for longer time than 2κ (i.e. > 6.08 h), the joint temperature is expected to have reached an equilibrium. Only data related to the expected thermal equilibrium was considered for the analysis.

3.2 Joint angles

Due to asymmetries in the contact surfaces, it has been observed that the friction of rotating machines depends on the angular position [2]. It is therefore expected that this dependency occurs also in a robot joint. Following the experiment guidelines from the previous section, a total of 50 static friction curves were estimated in the joint angle range $\varphi_a = [8.40, 59.00]$ deg. As seen in Fig. 7(a), little effects can be observed. The subtle deviations are comparable to the errors of the friction curve identified under constant values of $[\varphi_a, \tau_p, \tau_m, T]$. In fact, even a constant instance of $\mathcal{M}_0$ can describe the friction curves satisfactorily, no extra terms are thus required.

3.3 Joint load torque

Since friction is related to the interaction between contacting surfaces, one of the first phenomena observed was

[5] An ABB internal tool was used for simulation purposes.

[6] In the studies, the robot gearbox was lubricated with oil, not grease, which gave an opportunity to obtain well defined temperature readings by having a temperature sensor in the circulating lubricant oil.

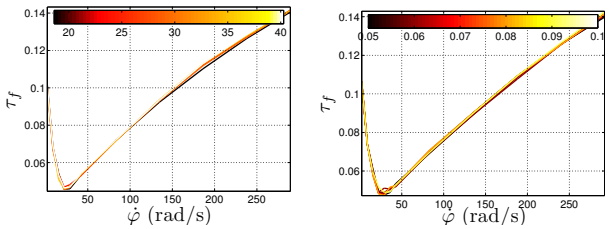

(a) Effects of φ_a at $\tau_m = -0.39$, $T = 34^\circ$C. (b) Effects of τ_p at $\tau_m = -0.39$, $T = 36^\circ$C.

Fig. 7. Static friction curves for experiments related to φ_a and τ_p.

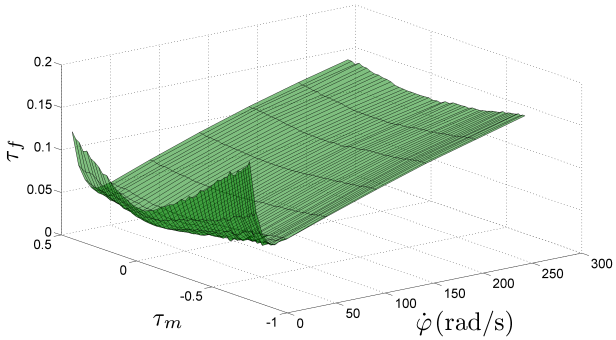

(a) Estimated friction curves for different values of τ_m.

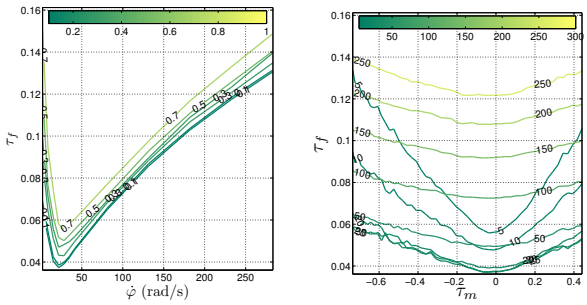

(b) Friction surface cuts for different values of τ_m.

(c) Friction surface cuts for different values of $\dot{\varphi}$ rad/s.

Fig. 8. The dependence of the static friction curves on the manipulation torque, τ_m, at $T = 34^\circ$C.

that friction varies according to the applied normal force. The observation is thought to be caused by the increase of the true contact area between the surfaces under large normal forces. A similar reasoning can be extended to joint torques in a robot revolute joint. Due to the elaborated joint gear- and bearing design it is also expected that torques in different directions will have different effects on the static friction curve[7].

Only small variations of τ_p, the perpendicular load torque, are achievable because of the mechanical construction of the robot, see Fig. 6(b). A total of 20 experiments at constant temperature were performed for joint 2, in the range $\tau_p = [0.04, 0.10]$. As Fig. 7(b) shows, the influences of τ_p for the achievable range did not play a significant role for the static friction curve. The model $\mathcal{M}_0$ is thus considered valid over the achieved range of τ_p for this joint.

Large variations of τ_m, the manipulation torque, are possible by simply varying the arm configuration, as seen in Fig. 6(a). A total of 50 static friction curves were estimated over the range $\tau_m = [-0.73, 0.44]$. As seen in Fig. 8, the effects appear clearly. Obviously, a single $\mathcal{M}_0$ instance can not describe the observed phenomena. A careful analysis of the effects reveals that the main changes occur in the velocity weakening part of the curve. From Fig. 8(c), it is possible to observe a (linear) bias-like (F_c) increase and a (linear) increase of the standstill friction (F_s) with $|\tau_m|$. Furthermore, as seen in Fig. 8(b), the Stribeck velocity $\dot{\varphi}$ is maintained fairly constant. The observations support an extension of $\mathcal{M}_0$ to

$$\tau_f(\dot{\varphi}, \tau_m) = \{F_{c,0} + F_{c,\tau_m}|\tau_m|\} + \\ + \{F_{s,0} + F_{s,\tau_m}|\tau_m|\} e^{-\left|\frac{\dot{\varphi}}{\dot{\varphi}_{s,\tau_m}}\right|^{\alpha^*}} + F_v\dot{\varphi}. \qquad (\mathcal{M}_1)$$

In the above equation, the parameters are written with subscript $_0$ or $_{\tau_m}$ in order to clarify its origin related to $\mathcal{M}_0$ or to the effects of τ_m. The model structure $\mathcal{M}_1$ is similar to the one presented in [28], where the changes in F_c and F_s appear as linear functions of $|\tau_m|$.

Assuming that any phenomenon not related to τ_m is constant and such that the $_0$ terms can capture them, good estimates of the τ_m-dependent parameters can be achieved. The model $\mathcal{M}_1$ is identified with the data set from Fig. 8 using the procedure described in Section 2.2. The resulting model parameters describing the dependence on τ_m are shown in Table 2.

Table 2. Identified τ_m-dependent model parameters.

$F_{c,\tau_m}\,[10^{-2}]$	$F_{s,\tau_m}\,[10^{-1}]$	$\dot{\varphi}_{s,\tau_m}$
2.34 ± 0.071	1.26 ± 0.025	9.22 ± 0.12

3.4 Temperature

The friction temperature dependence is related to the change of properties of both lubricant and contacting surfaces. In lubricated mechanisms, both the thickness of the lubricant layer and its viscosity play an important role for the resulting friction properties. In Newtonian fluids, the shear forces are directly proportional to the viscosity which, in turn, varies with temperature [31]. Dedicated experiments were made to analyze temperature effects. The joint was at first warmed up to 81.2°C by running the joint continuously back and forth. Then, while the robot cooled, 50 static friction curves were estimated over the range $T = [38.00, 81.20]^\circ$C. In order to resolve combined effects of T and τ_m, two manipulation torque levels were used, $\tau_m = -0.02$, and $\tau_m = -0.72$. As it can be seen in

[7] In fact, a full joint load description would require 3 torque and 3 force components.

Fig. 9, the effects of T are significant.

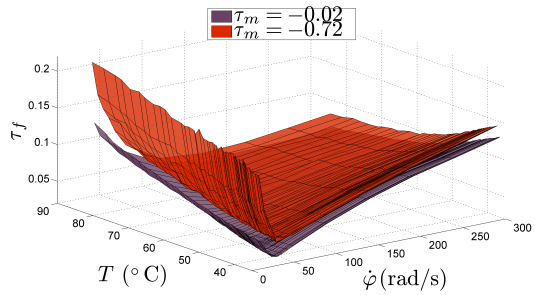

(a) Estimated friction curves for different values of T.

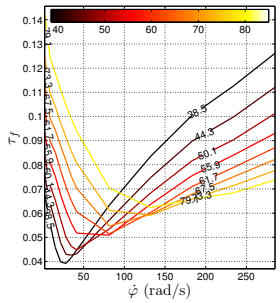

(b) Friction surface cuts for different values of T at $\tau_m = -0.02$.

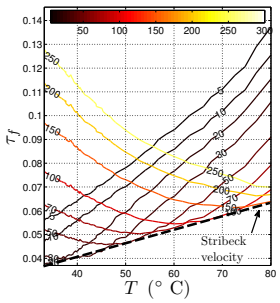

(c) Friction surface cuts for different values of $\dot{\varphi}$ rad/s at $\tau_m = -0.02$.

Fig. 9. The temperature dependence of the static friction curve.

Temperature has an influence on both velocity regions of the static friction curves. In the velocity-weakening region, a (linear) increase of the standstill friction (F_s) with temperature can be observed according to Fig. 9(b). In Fig. 9(c) it can moreover be seen that the Stribeck velocity ($\dot{\varphi}_s$) increases (linearly) with temperature. The effects in the velocity-strengthening region appear as a (nonlinear, exponential-like) decrease of the velocity-dependent slope, as seen in Fig. 9(b) and 9(c).

Combined effects of τ_m and T are also interesting to study. To better see these effects, the friction surfaces in Fig. 9(a) are subtracted from each other, yielding $\tilde{\tau}_f$. As it can be seen in Fig. 10(a), the result is fairly temperature independent. This is an indication of *independence between effects caused by T and τ_m*.

Given that the effects of T and τ_m are independent, it is possible to subtract the τ_m-effects from the surfaces in Fig. 9(a) and solely obtain temperature related phenomena. The previously proposed terms to describe the τ_m-effects in $\mathcal{M}_1$ were:

$$\hat{\tau}_f(\tau_m) = F_{c,\tau_m}|\tau_m| + F_{s,\tau_m}|\tau_m| e^{-\left|\frac{\dot{\varphi}_m}{\dot{\varphi}_{s,\tau_m}}\right|^{\alpha^*}}. \qquad (14)$$

With the parameter values given from Table 2, the manipulation torque effects were subtracted from the friction curves of the two surfaces in Fig. 9(a), that is, the quantities $\tau_f - \hat{\tau}_f(\tau_m)$ were computed. The resulting surfaces are shown in Fig. 10(b). As expected, the surfaces become quite similar. The result can also be interpreted as an evidence of the fact that the model structure used for the τ_m-dependent terms and the identified parameter values are correct. Obviously, the original model structure $\mathcal{M}_0$ can not

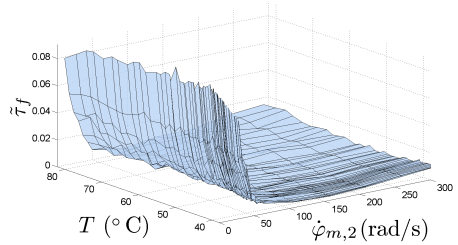

(a) Difference $\tilde{\tau}_f$ between the two static friction surfaces in Fig. 9(a).

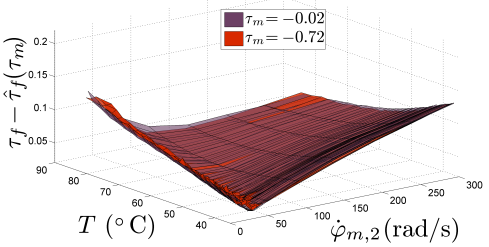

(b) Static friction surfaces in Fig. 9(a) after subtraction of the τ_m-dependent terms.

Fig. 10. Indication of independence between effects caused by T and τ_m.

characterize all observed phenomena, even after discounting the τ_m-dependent terms.

3.5 A proposal for $\mathcal{M}^*$

From the characteristics of the T-related effects and the already discussed τ_m-effects, $\mathcal{M}_1$ is extended to:

$$\begin{aligned}
&\tau_f(\dot{\varphi}, \tau_m, T) = \\
&\{F_{c,0} + F_{c,\tau_m}|\tau_m|\} + F_{s,\tau_m}|\tau_m| e^{-\left|\frac{\dot{\varphi}_m}{\dot{\varphi}_{s,\tau_m}}\right|^{\alpha^*}} + && (\mathcal{M}^*_{g,\tau_m}) \\
&+ \{F_{s,0} + F_{s,T}T\} e^{-\left|\frac{\dot{\varphi}_m}{\{\dot{\varphi}_{s,0} + \dot{\varphi}_{s,T}T\}}\right|^{\alpha^*}} + && (\mathcal{M}^*_{g,T}) \\
&+ \{F_{v,0} + F_{v,T} e^{\frac{-T}{T_{Vo}}}\}\dot{\varphi}. && (\mathcal{M}^*_{h,T})
\end{aligned}$$

The model describes the effects of τ_m and T for the investigated robot joint. The first $\mathcal{M}^*_g$ expressions relate to the velocity-weakening friction while $\mathcal{M}^*_h$ relates to the velocity-strengthening regime. τ_m only affects the velocity-weakening regime and requires a total of 3 parameters, $[F_{c,\tau_m}, F_{s,\tau_m}, \dot{\varphi}_{s,\tau_m}]$. T affects both regimes and requires 4

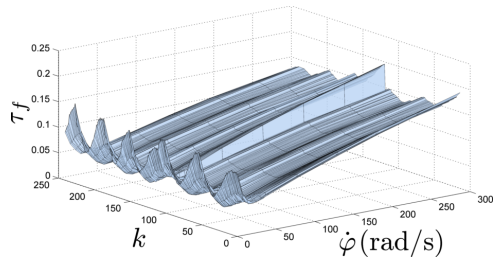

(a) Static friction curves.

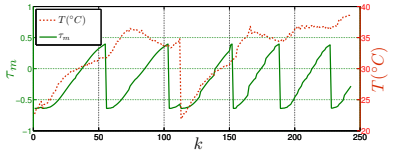

(b) τ_m- and T conditions.

Fig. 11. Validation data set. Notice the large variations of T- and τ_m values in Fig. (b) when registering the static friction curves in (a).

parameters, $[F_{s,T},\ \dot{\varphi}_{s,T},\ F_{v,T},\ T_{\mathrm{Vo}}]$. The 4 remaining parameters, $[F_{c,0},\ F_{s,0},\ \dot{\varphi}_{s,0},\ F_{v,0}]$, relate to the original friction model structure $\mathcal{M}_0$. Notice that under the assumption that τ_m- and T effects are independent, their respective expressions appear as separated sums in $\mathcal{M}^*$.

The term $F_{v,T}e^{-T/T_{\mathrm{Vo}}}$ in $\mathcal{M}^*_{h,T}$ is motivated by the exponential-like behavior of viscous friction (recall Fig. 9(c)). In fact, the parameter T_{Vo} is a reference to the Vogel-Fulcher-Tamman exponential description of viscosity and temperature [31]. Such behavior is observed in a large but limited temperature range, to capture the static friction behavior at even larger temperature ranges, more complex expressions may be needed, see [31] for other structures.

Given the already identified τ_m-dependent parameters in Table 2, the remaining parameters from $\mathcal{M}^*$ are identified from the measurement results presented in Fig. 10(b), after the subtraction of the τ_m-terms. The values are shown in Table 3.

3.6 Validation

A separate data set is used for the validation of the proposed model structure $\mathcal{M}^*$. It consists of several static friction curves measured at different τ_m- and T values, as seen in Fig. 11. With an instance of $\mathcal{M}^*$ given by the parameter values from Tables 2 and 3, the resulting distribution of the prediction errors, $p(\varepsilon)$, for the validation data set are shown in Fig. 12. As a comparison, the errors distribution related to a single instance of $\mathcal{M}_0$, with parameters given in Table 1, are also shown in the figure. As it can be seen, $\mathcal{M}^*$ is able to capture considerably more of the friction behavior than $\mathcal{M}_0$, with only speed dependence. The mean, standard deviation and largest absolute error for $\mathcal{M}^*$ are $[-9.24\,10^{-4}, 4.23\,10^{-3}, 1.88\,10^{-2}]$, compared to $[1.09\,10^{-2}, 1.34\,10^{-2}, 7.58\,10^{-2}]$ for $\mathcal{M}_0$.

The proposed model structure has also been successfully validated in other joints with similar gearboxes, but it might be interesting to validate it in other robot types and even other

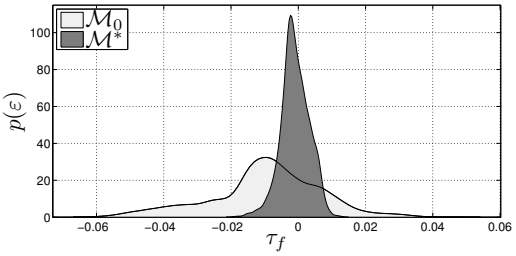

Fig. 12. Models prediction error distribution. Notice the considerable better performance of $\mathcal{M}^*$.

types of rotating mechanisms.

4 CONCLUSIONS AND FURTHER RESEARCH

The main contribution of this paper is the empirically derived model of static friction as a function of the variables $\mathcal{X}^* = [\dot{\varphi}, \varphi_a, \tau_p, \tau_m, T]$. While no significant influences of joint angle and perpendicular torque could be found by the experiments, the effects of manipulation torque, τ_m, and temperature, T, were significant and included in the proposed model structure $\mathcal{M}^*$. As shown in Fig. 12 the model is needed in applications where the manipulation torque and the temperature play significant roles. For example in [10], the model structure $\mathcal{M}^*$ was used to design a diagnosis routine that infers the wear levels of a gearbox from friction observations under temperature uncertainties.

In the studies, the friction phenomena was fairly direction independent. If this was not the case, two instances of $\mathcal{M}^*$ could be used to describe the whole speed range, but requiring two times more parameters. The model $\mathcal{M}^*$ has a total of 7 terms and 4 parameters which enter the model in a nonlinear fashion. The identification of such a model is computationally costly and requires data from several different operating conditions. Studies on defining sound identification excitation routines are therefore important.

Only static friction (measured when transients caused by velocity changes have disappeared) was considered in the studies. It would be interesting to investigate if a dynamic model, for instance given by the LuGre model structure $\mathcal{M}_L$, could be used to describe dynamic friction with extensions from the proposed $\mathcal{M}^*$. However, to make experiments on a robot joint in order to obtain a dynamic friction model is a big challenge. Probably, such experiments must be made on a robot joint mounted in a test bench instead of on a robot arm system, which has very complex dynamics.

A practical limitation of $\mathcal{M}^*$ is the requirement on availability of τ_m and T. Up to date, torque- and joint temperature sensors are not available in standard industrial robots. As mentioned in Section 3.1, the joint torque components can still be estimated from the torque reference to the drive system by means of an accurate robot model. In this situation, it is important to have correct load parameters in the model to calculate the load torque components.

Regardless these experimental challenges, there is a great potential for the use of $\mathcal{M}^*$ for simulation-, design-

Table 3. Identified T-dependent and $\mathcal{M}_0$-related model parameters.

$F_{c,0}\,[10^{-2}]$	$F_{s,0}\,[10^{-2}]$	$F_{s,T}\,[10^{-3}]$	$F_{v,0}\,[10^{-4}]$	$F_{v,T}\,[10^{-3}]$	$\dot{\varphi}_{s,0}$	$\dot{\varphi}_{s,T}$	T_{Vo}
3.11 ± 0.028	-2.50 ± 0.12	1.60 ± 0.022	1.30 ± 0.056	1.32 ± 0.076	-24.81 ± 0.87	0.98 ± 0.018	20.71 ± 0.91

and evaluation purposes. The designer of control algorithms, the diagnosis engineer, the gearbox manufacturer, etc. would benefit by using a more realistic friction model.

References

[1] Golub, G. H., and Pereyra, V., 1973. "The differentiation of pseudo-inverses and nonlinear least squares problems whose variables separate". *SIAM Journal on Numerical Analysis,* **10**(2), pp. pp. 413–432.

[2] Al-Bender, F., and Swevers, J., 2008. "Characterization of friction force dynamics". *IEEE Control Systems Magazine,* **28**(6), pp. 64–81.

[3] Dowson, D., 1998. *History of Tribology*. Professional Engineering Publishing, London, UK.

[4] Kim, H. M., Park, S. H., and Han, S. I., 2009. "Precise friction control for the nonlinear friction system using the friction state observer and sliding mode control with recurrent fuzzy neural networks". *Mechatronics,* **19**(6), pp. 805 – 815.

[5] Guo, Y., Qu, Z., Braiman, Y., Zhang, Z., and Barhen, J., 2008. "Nanotribology and nanoscale friction". *Control Systems Magazine, IEEE,* **28**(6), dec., pp. 92 –100.

[6] Olsson, H., Åström, K. J., de Wit, C. C., Gafvert, M., and Lischinsky, P., 1998. "Friction models and friction compensation". *European Journal of Control,* **4**(3), pp. 176–195.

[7] Bona, B., and Indri, M., 2005. "Friction compensation in robotics: an overview". In Decision and Control, 2005. Proceedings., 44th IEEE International Conference on.

[8] Witono Susanto, Robert Babuska, F. L., and van der Weiden, T., 2008. "Adaptive friction compensation: application to a robotic manipulator". In The International Federation of Automatic Control, 2008. Proceedings., 17th World Congress.

[9] Blau, P. J., 2009. "Embedding wear models into friction models". *Tribology Letters,* **34**(1), Apr.

[10] Bittencourt, A., Axelsson, P., Jung, Y., and Brogårdh, T., 2011. "Modeling and identification of wear in a robot joint under temperature uncertainties". In In IFAC World Congress.

[11] Caccavale, F., Cilibrizzi, P., Pierri, F., and Villani, L., 2009. "Actuators fault diagnosis for robot manipulators with uncertain model". *Control Engineering Practice,* **17**(1), pp. 146 – 157.

[12] Namvar, M., and Aghili, F., 2009. "Failure detection and isolation in robotic manipulators using joint torque sensors". *Robotica*.

[13] McIntyre, M., Dixon, W., Dawson, D., and Walker, I., 2005. "Fault identification for robot manipulators". *Robotics, IEEE Transactions on,* **21**(5), Oct., pp. 1028–1034.

[14] Vemuri, A. T., and Polycarpou, M. M., 2004. "A methodology for fault diagnosis in robotic systems using neural networks". *Robotica,* **22**(04), pp. 419–438.

[15] Brambilla, D., Capisani, L., Ferrara, A., and Pisu, P., 2008. "Fault detection for robot manipulators via second-order sliding modes". *Industrial Electronics, IEEE Transactions on,* **55**(11), Nov., pp. 3954–3963.

[16] Mattone, R., and Luca, A. D., 2009. "Relaxed fault detection and isolation: An application to a nonlinear case study". *Automatica,* **42**(1), pp. 109 – 116.

[17] Freyermuth, B., 1991. "An approach to model based fault diagnosis of industrial robots". In Robotics and Automation, 1991. Proceedings., 1991 IEEE International Conference on, Vol. 2, pp. 1350–1356.

[18] Waiboer, R., 2007. "Dynamic modelling, identification and simulation of industrial robots". PhD thesis, University of Twente.

[19] Armstrong-Hélouvry, B., 1991. *Control of Machines with Friction*. Kluwer Academic Publishers.

[20] Åström, K. J., and Canudas-de Wit, C., 2008. "Revisiting the lugre friction model". *Control Systems Magazine, IEEE,* **28**(6), Dec., pp. 101–114.

[21] Avraham Harnoy, B. F. S. C., 2008. "Modeling and measuring friction effects". *Control Systems Magazine, IEEE,* **28**(6), Dec.

[22] Jacobson, B., 2003. "The stribeck memorial lecture". *Tribology International,* **36**(11), pp. 781 – 789.

[23] Woydt, M., and Wäsche, R., 2010. "The history of the stribeck curve and ball bearing steels: The role of adolf martens". *Wear,* **268**(11-12), pp. 1542 – 1546.

[24] Bo, L. C., and Pavelescu, D., 1982. "The friction-speed relation and its influence on the critical velocity of stick-slip motion". *Wear,* **82**(3), pp. 277 – 289.

[25] Waiboer, R., Aarts, R., and Jonker, B., 2005. "Velocity dependence of joint friction in robotic manipulators with gear transmissions". In Proceedings of the ECCOMAS Thematic Conference Multibody Dynamics 2005, pp. 1–19.

[26] Gogoussis, A., and Donath, M., 1988. "Coulomb friction effects on the dynamics of bearings and transmissions in precision robot mechanisms". In Robotics and Automation, 1988. Proceedings., 1988 IEEE International Conference on, pp. 1440 –1446 vol.3.

[27] Dohring, M., Lee, E., and Newman, W., 1993. "A load-dependent transmission friction model: theory and experiments". In Robotics and Automation, 1993. Proceedings., 1993 IEEE International Conference on, pp. 430 –436 vol.3.

[28] Hamon, P., Gautier, M., and Garrec, P., 2010. "Dynamic identification of robots with a dry friction model depending on load and velocity". In Intelligent Robots and Systems (IROS), 2010 IEEE/RSJ International Conference on, pp. 6187 –6193.

[29] Bittencourt, A., Wernholt, E., Sander-Tavallaey, S., and Brogårdh, T., 2010. "An extended friction model to capture load and temperature effects in robot joints". In Intelligent Robots and Systems (IROS), 2010 IEEE/RSJ International Conference on, pp. 6161 –6167.

[30] Ljung, L., 1998. *System Identification: Theory for the User (2nd Edition)*. Prentice Hall PTR, December.

[31] Seeton, C. J., 2006. "Viscosity-temperature correlation for liquids". *Tribology Letters,* **22**(1), Mar., pp. 67–78.